Effect of Synthesis Conditions on Pseudocapacitance Properties of Nitrogen-Doped Porous Carbon Materials

Article *in* Journal of Nano Research · August 2019

DOI: 10.4028/www.scientific.net/JNanoR.59.112

CITATIONS
0

READS
45

7 authors, including:

V. O. Kotsyubynsky
Vasyl Stefanyk Precarpathian National University
72 PUBLICATIONS **68** CITATIONS
SEE PROFILE

Andrii Kachmar
Vasyl Stefanyk Precarpathian National University
8 PUBLICATIONS **3** CITATIONS
SEE PROFILE

Sergiy Budzulyak
National Academy of Sciences of Ukraine
60 PUBLICATIONS **42** CITATIONS
SEE PROFILE

B. I. Rachiy
Vasyl Stefanyk Precarpathian National University
41 PUBLICATIONS **74** CITATIONS
SEE PROFILE

Journal of Nano Research
ISSN: 1661-9897, Vol. 59, pp 112-125

Submitted: 2019-02-11
Revised: 2019-06-18
Accepted: 2019-06-20
Online: 2019-08-27

Effect of Synthesis Conditions on Pseudocapacitance Properties of Nitrogen-Doped Porous Carbon Materials

Volodymyr Boichuk[1,a], Volodymyr Kotsyubynsky[2,b*], Andrii Kachmar[3,c], Sergiy Budzulyak[4,d], Ivan Budzulyak[5,e], Bogdan Rachiy[6,f], Lyubov Yablon[7,g]

[1,2,3,5,6,7]Vasyl Stefanyk PreCarpathian National University,
57 Shevchenko Str., Ivano-Frankivsk, 76018, Ukraine

[4]V.E. Lashkaryov Institute of Semiconductor Physics, NAS of Ukraine,
41 Nauky str., Kyiv, 03028, Ukraine

[a]vmbojchuk@gmail.com, [b]kotsuybynsky@gmail.com, [c]andrij.nj@gmail.com, [d]buser@ukr.net,
[e]ivan-budzulyak@ukr.net, [f]bogdan_rachiy@ukr.net, [g]yablon_lyubov@ukr.net

Keywords: Supercapacitor; Nitrogen-doped carbon; Pseudocapacitance; Raman spectroscopy; Impedance spectroscopy.

Abstract. The electrochemical properties of the nitrogen-enriched carbons obtained by plant raw treatment as electrode material for supercapacitors were investigated by electrochemical impedance spectroscopy, cycling voltammetry and galvanostatic charge-discharge cycling in KOH aqueous electrolyte. The effect of activation agent (NaOH) concentration and carbonization temperature were analyzed. The separation of double layer and redox capacitance components was done. The dominating role of microporosity for capacitive properties was demonstrated. The capacitance of model capacitors based on carbons obtained at different modes was calculated from both from cycling voltammetry and galvanostatic charge-discharge data. The maximal values of specific capacitance of carbon materials carbonized at 600ºC and 900ºC are about 100 and 120 F/g, respectively.

1. Introduction

There are two different energy storage mechanisms for electrochemical supercapacitors – pure electrostatic one with the electrical double layer formation on the electrode-electrolyte interface [1] and pseudocapacitance developed as a result of reversible surface redox processes [2-4]. Hybrid electrode material that combines electronic conductivity, high specific surface area and also redox activity have a great potential [5-7]. Composite and hybrid materials on the base of graphene and ultrafine transition metals oxides, hydroxides or selenides are the most promising [8-11]. Another effective strategy to improve the catalytic and electrochemical performance of carbon materials is their doping with nitrogen [12]. Nitrogen-doped porous carbon nanomaterials have new technological applications, for example cathode catalyst for fuel cells with excellent oxygen reduction electrocatalytic activity [13]. At the same time N-doped activated carbons have good prospects for application in supercapacitors [14]. One of the reason of double layer capacitance improvement is the increasing of the surface positive charge density due to higher electronegativity of nitrogen with the simultanenous increasing of surface wettability [15]. The presence of surface-decorated polar functional groups increases an affinity to polar solvents that is very important for using of aqueous electrolyte with economical and environmental advantages.

Another important reason is the enlarging of microporous carbon's electrical conductivity after nitrogen atoms introduction doping of an additional electron into the delocalized π-system of the graphite-like fragments [16]. At the same time the nitrogen doping caused the distortion of the crystal lattice of graphite fragments that leads to decreasing of electrical conductivity, so controlling of nitrogen concentration is critically important for obtaining the materials with high electrochemical performance [16]. Besides, the presence of nitrogen functional groups on the carbon surface induces the redox reactions and causes the pseudocapacitance properties appearance [17].

The most probable mechanism of faradaic reactions on the N-doped carbon surface involves the participitation of protons and pyridinic-type nitrogen or pyrrolic-type nitrogen groups [18]. The combination of two ways of charge storage mechanism – the electric double-layer capacitance with pseudocapacitance allows to obtain low-cost materials with high specific capacitance at high charge-discharge rates [19]. While the progress in these areas depends on the development of highly effective methods of N-doped carbons production with controlled morphological properties and electrochemical performance.

2. Materials and Characterization

The microporous carbon was obtained on the base of plant feedstock using carbonization and chemical activation. The dry apricot pit shells (fraction size of about 0.25-1 mm) were carbonized in the high pressure reactor at 600 and 900 °C. Apricot pit shells are a high effective lignocellulosic source and attractive material for pyrolysis and carbonization due to high carbon and low ash contents [20]. The choice of applied carbonization temperatures values (600 and 900ºC) was based on the thermal analysis of raw materials (apricot pit shells) in the temperature range of 20-1000ºC (Fig.1).

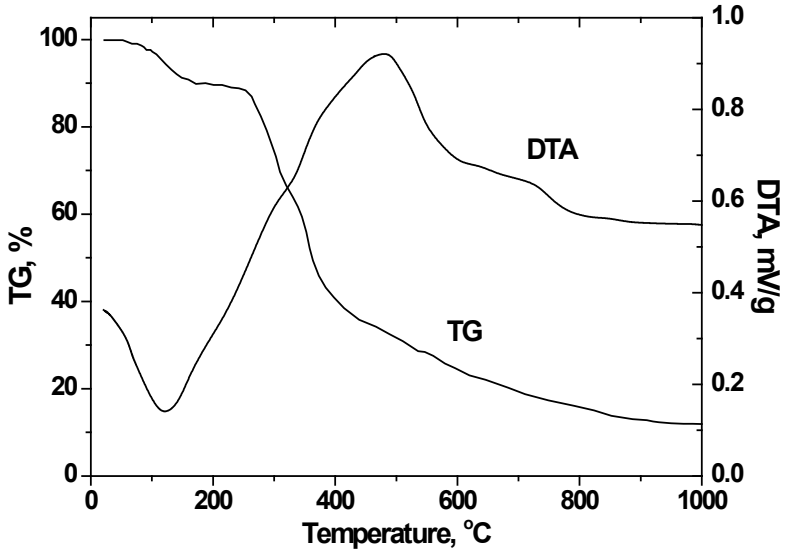

Fig.1. The results of thermogravimetric / differential thermal analysis of raw material (apricot pit shells).

The intensive mass loss finished at about 380ºC. The final decomposition of hemicellulose and cellulose occurs at the temperatures up to 600 C when lignin pyrolysis continues to about 900ºC [21]. The materials obtained after carbonization procedure were milled until the fraction size of about 200-250 μm and mixed with sodium hydroxide and distilled water. Weight ratio of m(NaOH):m(C) values were 0.25, 0.5, 0.75 and 1 under the condition that mass of water equals to the mass of carbon. The resulting mixtures were stirred for 2 hours, dried to the constant weight at 90 °C and annealed in argon atmosphere at 600 °C (heating rate of 10 °C/min) for 20 min. The obtained powders were mixed with HNO_3 as nitrogen source under the continuous stirring at 50 °C in N_2 flow. Nitrogen concentrations in carbon samples were determined by elemental analysis using an Quantax (Bruker Nano GmbH) EDS system for VEGA 3 TESCAN Scanning Electron Microscope. Typical result of EDS spectroscopy of the as-synthesized nitrogen doped carbon samples are shown in Fig.2. It is determined the average nitrogen content is close to 2.9±0.3 wt. % for all the samples. This values were selected corresponding to the results of [16] where the maximal electrical conductivity of N-doped carbon nanofiber was observed at nitrogen concentration of about 3.1 wt. %. The synthesized materials were washed to neutral pH and dried at 90 °C up to constant weight. Average nitrogen content in carbons was about 1.5-2.0 wt. %. The activation procedure was repeated for selected samples.

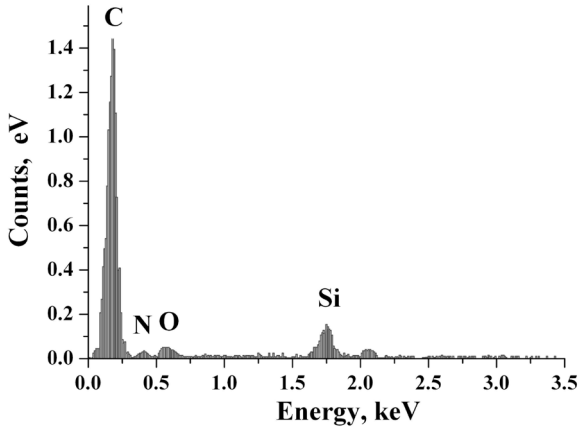

Fig. 2. Typical EDS spectra of N-doped microporous carbon.

The obtained mesoporous carbons (MC) were marked according to m(NaOH):m(C) ratio value, the carbonization temperature value and the number of activation procedures. For example, MC-025-600-1 is a material obtained at m(NaOH):m(C) ratio value equals to 0.25 using carbon prepared at 600 °C with the activation number equal to 1. The conditions of samples obtaining are summarized in Table 1.

Table 1. The synthesis details and porous structure characteristics of carbon samples

Sample	S_{BET}, [m^2/g]	S_{micro}, [m^2/g]	V_{micro}, [cm^3/g]	S_{meso}, [m^2/g]	V_{total}, [cm^3/g]
MC-025-600-1	268	268	0.06	–	0.06
MC-050-600-1	320	320	0.08	–	0.08
MC-075-600-1	423	423	0.12	–	0.12
MC-100-600-1	408	377	0.16	31	0.18
MC-075-600-2	417	395	0.12	22	0.13
MC-100-600-2	379	289	0.14	90	0.21
MC-025-900-1	168	132	0.07	36	0.10
MC-050-900-1	197	150	0.08	47	0.12
MC-075-900-1	321	215	0.11	106	0.20
MC-100-900-1	582	551	0.23	31	0.25
MC-075-900-2	351	250	0.12	101	0.20
MC-100-900-2	566	520	0.22	46	0.25

The specific surface area and pore size distribution of MC samples were analyzed using low temperature nitrogen adsorption/desorption (Quantachrome Autosorb Nova 2200e device). The carbon samples were degassed at 180 °C for 18 h before measuring of morphological characteristics. The specific surface area (S_{BET}, m^2/g) value was calculated by multipoint BET method [22]. The total pore volume (V_{total}, cm^3/g) was calculated by the number of adsorbed nitrogen [22]. The volume of micropores (V_{micro}, cm^3/g) and the values of specific surface of micro- (S_{micro}, m^2/g), and mesopores (S_{mezo}, m^2/g) were found using t-method [22].

Electrochemical investigations were carried out in a three-electrode cell with a reference Ag/AgCl electrode, platinum wire as a counter electrode and a working electrode on the pure Ni grid. Working electrode consists of 75 % active material and 25 % acetylene black as a conductive additive. Electrochemical performance was measured in 6 M KOH as an electrolyte. The specific capacitances were measured at specific currents in a range of 0.08-0.40 A/g. Cyclic voltammetry (CV) investigations were carried out at scan rate of 0.5, 1, 2, 3, 4 and 5 mV/s. Electrochemical impedance spectra (EIS) were measured at frequencies from 0.01 Hz up to 100 kHz. The measurements were carried out using Autolab PGSTAT12 (ECO CHEMIE Company) with GPES and FRA-2 software. All the measurements were carried out in the same type of three electrodes

electrochemical cell with Pt pseudo-reference electrode and Ag/AgCl reference electrode. Impedance measurements were carried out after the cyclic voltammetry studies in a constant voltage mode (0.2, 0.4, 0.6, 0.8, 1.0, 1.2 V vs Ag/AgCl). Zview2 analytic software was used for impedance spectroscopy data analysis [23]. The surface morphology of the obtained samples was investigated by a Tescan Vega-3 scanning electron microscope (SEM).

Raman spectra of synthesized nitrogen doped carbons were obtained in reverse scattering geometry using the argon-krypton laser source (excitation radiation wavelength of 488 nm) with T64000 Jobin-Yvon spectrometer. The irradiation power < 1mW/cm^2 was used to avoid the heat damage of the samples.

STA 449 F3 Jupiter (Netzsch) device was used for thermal analysis. The measurements were carried out in the argon atmosphere in the temperature range of 20-1000ºC.

3. Results and Discussion

Nitrogen adsorption/desorption isotherms for carbonized at 600 °C carbon samples after one activation procedure (Fig. 3.a) belong to I type of IUPAC classification indicating microporous solids regardless of m(NaOH):m(C) ratio during activation procedure. Simultaneously the total pore volume increases with the increasing of activation agent content (Fig. 3.a). At the same time adsorption/desorption isotherms for materials obtained using two activation procedures have the hysteresis loop that corresponds to H4-type of IUPAC classification and capillary polymolecular adsorption in micro- and mesopores (Fig. 3.b).

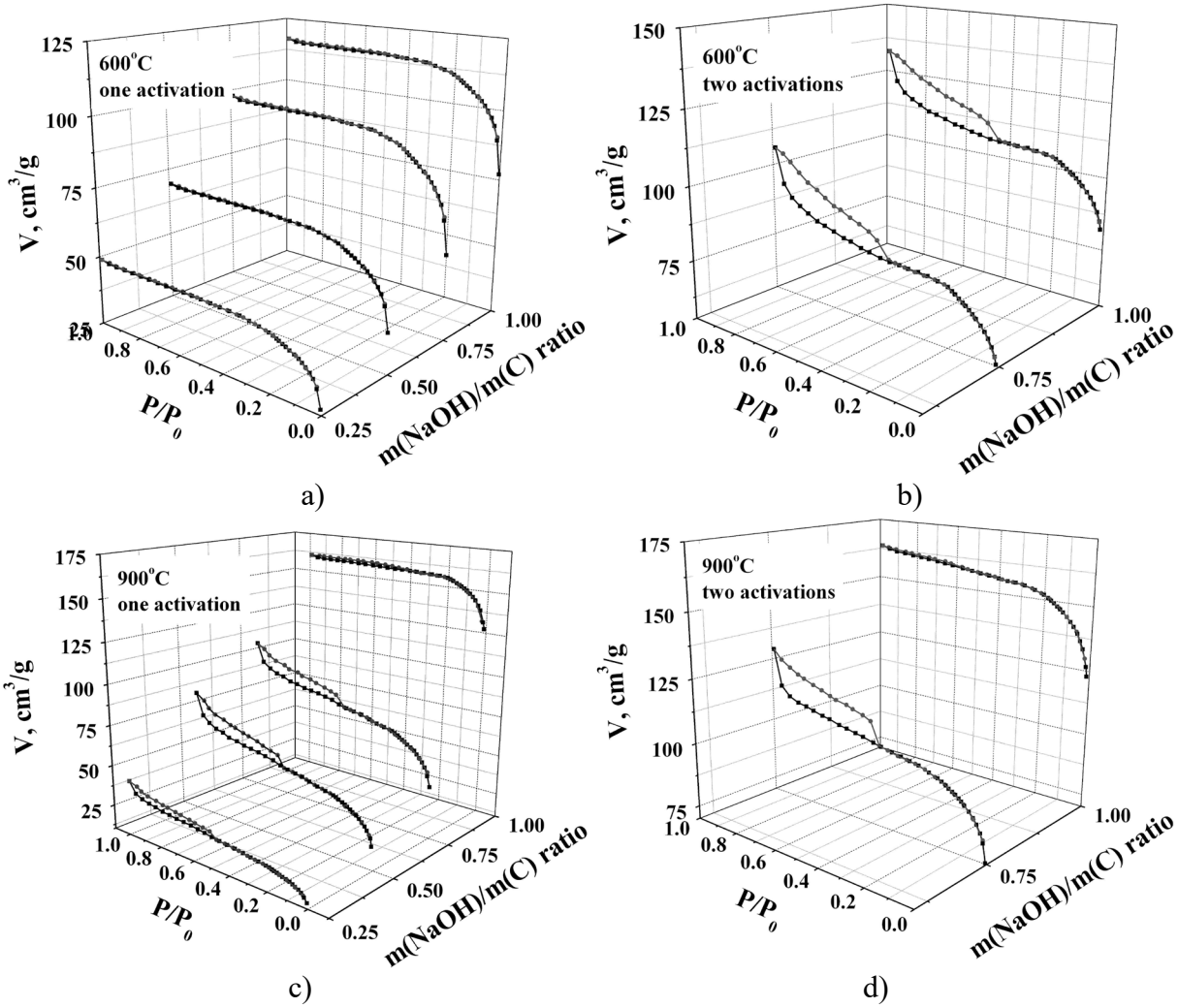

Fig. 3. Nitrogen adsorption/desorption isotherms for MC samples carbonized at 600 and 900 °C after one (a, c) and two (b, d) activation procedures respectively.

The increasing of hysteresis loop in adsorption/desorption isotherms for samples carbonized at 900 °C with one activation procedure is observed for increasing of m(NaOH):m(C) ratios in a range of 0.25 to 0.75 but material obtained at the maximal concentration of NaOH is characterized by decreasing of capillary condensation probability (Fig. 3.c). The same regularity was observed for the case of double activated samples prepared at 900 °C (Fig. 3.d).

The calculated values of specific surface area, average volumes of micro- and mesopores of all the synthesized samples are summarized in Table 1. The values of specific surface area for sample obtained at 600 °C vary in a range of 268-423 m^2/g in the case of one activation procedure with the tendency to increasing when NaOH concentration grows. This regularity was also observed for once activated samples obtained at 900 °C. The slight decreasing of BET specific surface area for double activated carbons in comparison with the once activated samples obtained at the same m(NaOH):m(C) ratios was observed independently on carbonization temperatures. MC-100-900-1 sample has a maximal (582 m^2/g) value of specific surface area.

Raman spectroscopy allows separating the response of graphitized part and non-graphitized part of carbon materials with complex microstructure. Raman spectra of the obtained materials contain two peaks at around 1580-1590 (G-band) and 1340-1360 cm^{-1} (D-band) The G band corresponds to doubly degenerate phonon mode for E_{2g} symmetry of sp^2 carbon networks and is an evidence of graphite structure presence. The complex D band corresponds to sp^3 carbon networks and its relative intensity grows with the enlarging of disordered carbon content. The ratio of I_D/I_G integrated intensity for the D and G bands can be used for characterizing of the graphitization degree of synthesized materials [24]. Raman spectra of the carbon materials obtained at different carbonization and activation conditions are (as shown in Fig.4) with the deconvolutions into Gauss band shapes after a baseline subtraction.

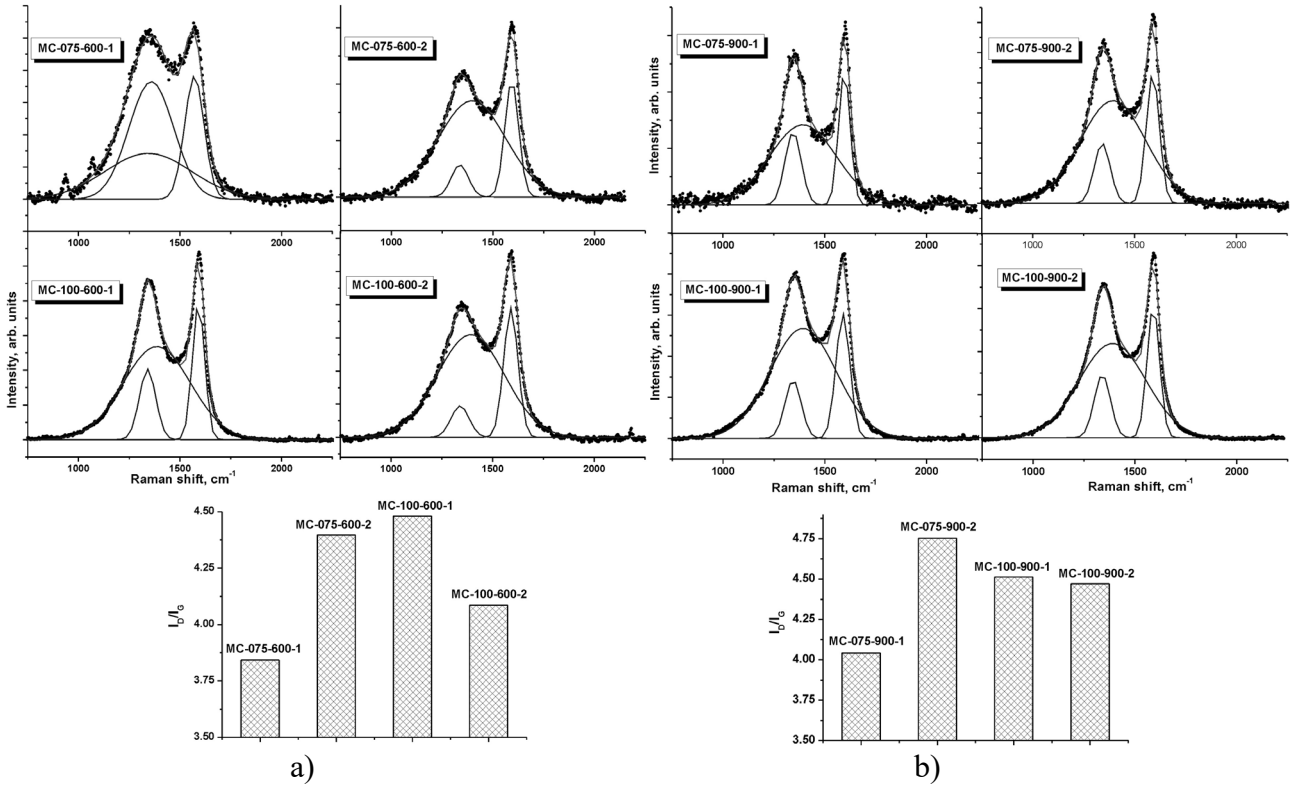

Fig. 4. Deconvoluted Raman spectra of the materials carbonized at (a) 600ºC and (b) 900ºC after activation under different conditions with the calculated ratio of the I_D/I_G bands integrated intensities.

All the spectra consist of relatively narrow G-band at about 1590-1593 cm^{-1} corresponding to in-plane optical mode at the center of the Brillouin zone and complex D-bands are assigned to non-ordered carbon. The optimal approximation of D-band was done using two components that appear

as a result of the π and π* electronic states splitting [25]. It is known that D-band for graphene has singlet-type, for two-layered graphene it is a quadruplet and for graphite-like packages with five and more layers D-band splitting merges into a doublet [26]. The components of D-band are associated with local unsymmetrical vibration of chemical bonds in graphitized defect carbon. The I_D/I_G ratio values that does not depend on the carbonization temperature are minimal for m(NaOH):m(C) weight ratio equals to 0.75, that corresponds to the maximal graphitization degree. It can be concluded that the second activation procedure causes the decreasing of graphitization degree for materials obtained under the condition of m(NaOH):m(C) = 0.75 and its increasing for carbon materials obtained at m(NaOH):m(C) weight ratio equals to 1. There is a linear dependency between (I_D/I_G) and $1/L_a$ [27]: $L_a\left(nm\right)=(2.4\times10^{-10})\lambda^4\left(\frac{I_D}{I_G}\right)^{-1}$, where L_a (nm) is an average crystallite size of graphite, λ (nm) is a laser line wavelength. The calculated values of graphite crystallite size for carbons obtained under different carbonization and activation conditions are presented in Fig.5. The double activation procedure at m(NaOH):m(C) = 0.75 for both used carbonization temperatures (600 and 900ºC) allows to obtain the carbon materials with the lowest average size of graphite nanocrystal.

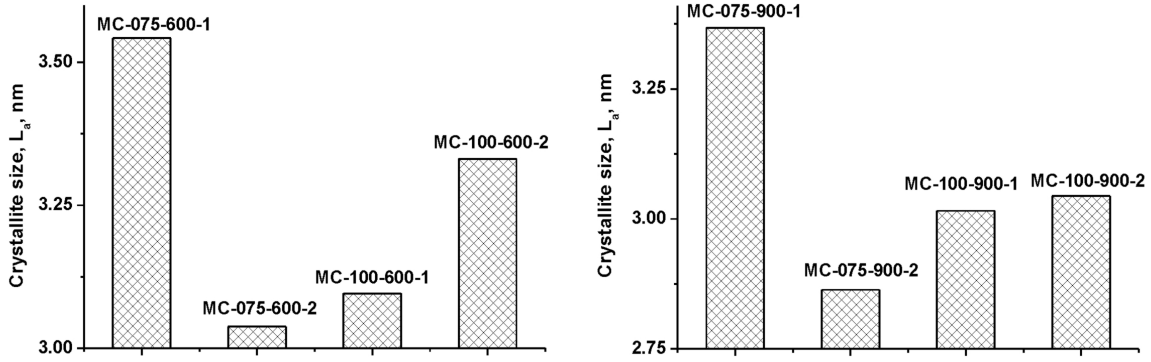

a) b)

Fig.5. The average crystallite size of graphite for carbon materials obtained after carbonization at (a) 600 and (b) 900ºC under different activation conditions

Nyquist plots for the samples obtained at 600 °C after one (Fig. 6.a, b) and two (Fig. 6.c, d) activation procedures were measured. It is known that electrochemical impedance spectra of porous carbon typically depend on three frequency-dependent processes probability [28]: the mass transfer is unlikely at high-frequencies so only charge transfer at the electrode/electrolyte interface contributes to system electrochemical response; the ion diffusion in mesoporous channels will be dominant for medium-frequencies; non-homogeneous diffusion in less-accessible sites will be important in low-frequency region.

Nyquist plots for samples obtained at 600 °C under the condition of one activation procedure consist of a small high-frequency semicircle (the result of limitations on H^+, Na^+, OH^- ion transport through the carbon) and a line close to straight at the low-frequency region (corresponds to the double-layer capacitance). It can be concluded that the charge transfer resistance through the electric double layer on the electrolyte/electrode interface within the electrode materials is relatively low and doesn't depend on the bias potential. The main reason for observed tendency to decreasing of internal resistance with the increasing of m(NaOH):m(C) ratio is the enlarging of penetration ability of carbon due to porosity increasing. The medium frequencies regions are characterized by the 45º Warburg segment that corresponds to diffusion process from the electrolyte into the carbon pores. The tendency to increasing of Warburg segment with the increasing of m(NaOH):m(C) ratio is observed that indicates an increase in Warburg resistance faced by the electrolyte ions during their transport. A pure capacitor should demonstrate a vertical line for low frequency region. The deviation from the expected behavior is an evidence of ion diffusion into the pores of carbon material and the pore size distribution of the porous matrix.

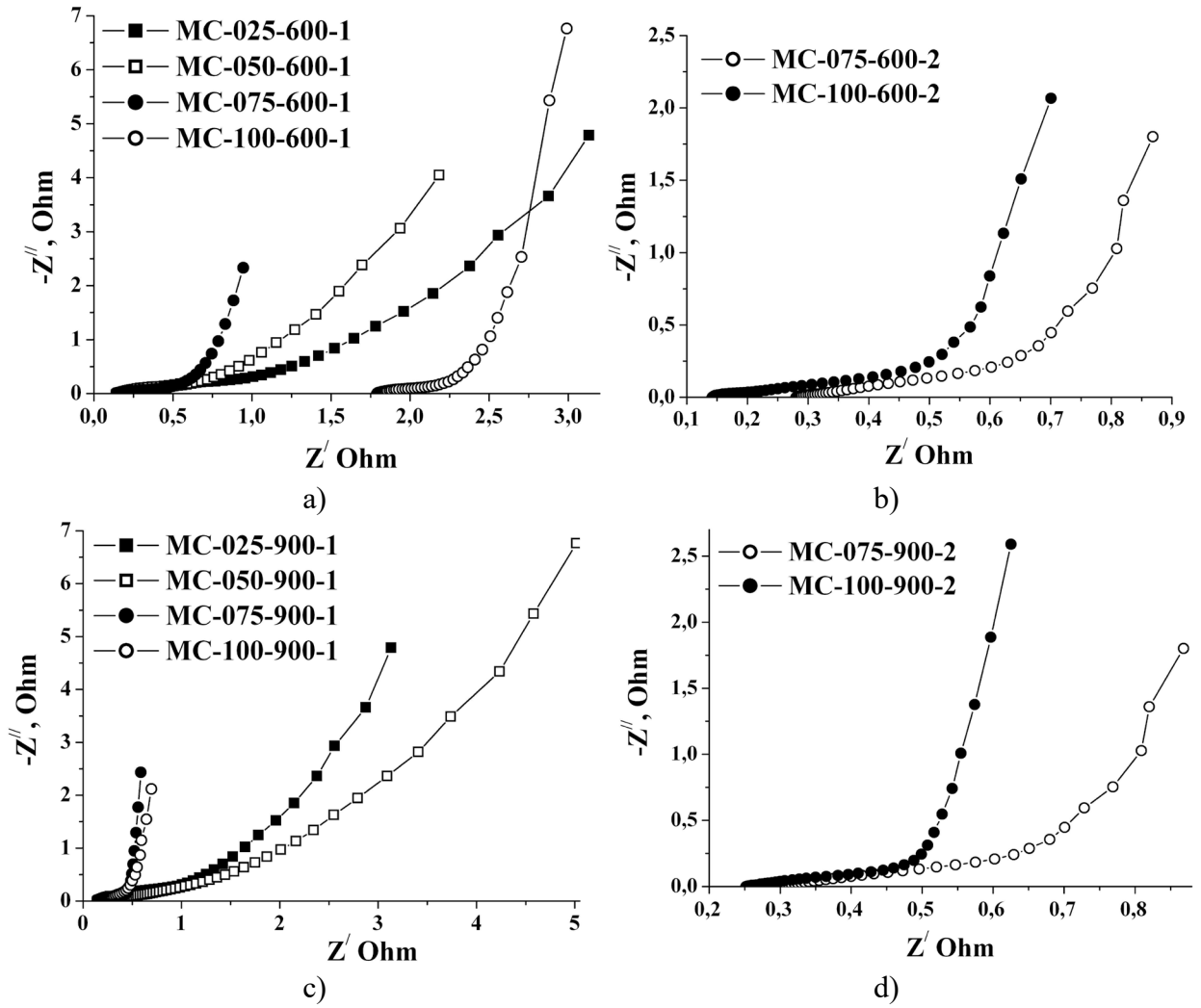

Fig. 6. Nyquist plots of MC samples carbonized at 600 and 900 °C after one (a, b) and two (c, d) activation procedures, respectively.

The equivalent circuit used for experimental impedance data fitting is presented in Fig. 7. The high and medium-frequency data were fitted with R_s-(R_1-CPE_1) chains, where R_s is the resistance of the electrolyte combined with the internal resistance of the electrode. The impedance of the constant phase element can be written as $Z_{CPE} = \frac{1}{T_{CPE}(i\omega)^{P_{CPE}}}$, where P_{CPE} is the constant phase exponent ($0 \leq P_{CPE} \leq 1$) and T_{CPE} is the capacitance when $P_{CPE} = 1$, the Warburg impedance when $P_{CPE} = 0.5$ and resistance when P_{CPE} close to 0.

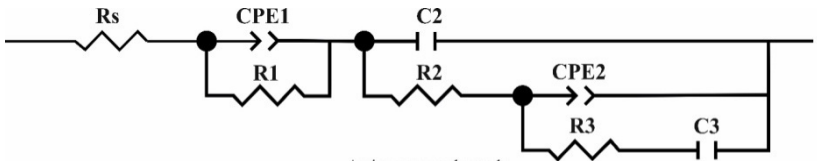

Fig. 7. Equivalent circuit for modeling the impedance MC samples.

In our case constant phase element CPE_1 is associated with the combination of the double-layer capacitance from the carbon and some pseudocapacitance component caused by Faradaic charge transfer processes. R_1 placed in parallel with CPE_1 is the leakage resistance corresponds to ion diffusion transfer through the electrode / electrolyte interface. The medium-and high frequency data were fitted using Randles-type circuit C_2-(R_2-CPE_2), where C_2-R_2 -chain represent the process of electric double layer formation in large micro- and mesopores: C_2 is homogeneously distributed capacity of EDL and R_2 is the resistance of this process. The chain CPE_2-(R_3-C_3) is associated with

diffusive ion transportation and corresponds to low-frequency Faradaic impedance caused by non-homogeneous ionic transport in micropores. The used approach is close to equivalent circuit proposed in [29].

The fitted data for circuit elements calculated for zero bias potential are generalized in Table 2. The Kramers-Kronig coefficient for fitting procedure does not exceed 8×10^{-4}; the difference between experimental and model curves does not exceed 10 %. It is important that the base equivalent circuit composition changes for samples obtained at different synthesis conditions. The charge transfer resistance R_1 corresponds to redox processes and charge transfer through the electrode/electrolyte interface is close to zero. The low values of R_1 can be associated with the presence of open morphology and good possibility for EDL formation. The values of R_1 resistance for samples with the mesopores presence are some higher that can be explained by the polymolecular absorption. Only low tendency to R_1 increasing for spectra obtained under more positive potential is observed (Fig. 6a).

Table 2. Fitted equivalent circuit elements of MC samples obtained under different conditions

Sample	Rs, [Ohm]	R_1, [Ohm]	CPE_1-T	CPE_1-P	CPE_2-T	CPE_2-P	R_3, [Ohm]	C_3, [mF]
MC-025-600-1	0.15	–	0.39	0.78	1.80	0.39	–	–
MC-050-600-1	0.10	–	0.96	0.95	2.68	0.43	–	4.98
MC-075-600-1	0.14	–	1.84	0.84	5.48	0.41	–	7.87
MC-100-600-1	1.78	0.52	2.44	0.89	3.67	0.45	2.03	1.26
MC-075-600-2	0.28	0.87	1.79	–	–	–	–	0.31
MC-100-600-2	0.13	–	2.31	0.88	12.86	0.38	–	–
MC-025-900-1	0.21	1.84	0.16	0.62	0.51	0.39	15.37	0.91
MC-050-900-1	0.24	2.54	0.31	0.70	0.79	0.45	13.96	–
MC-075-900-1	0.29	1.07	1.10	0.87	2.22	0.42	–	–
MC-100-900-1	0.16	–	2.62	0.82	22.20	0.36	–	9.42
MC-075-900-2	0.25	0.35	1.38	0.99	6.06	0.48	–	–
MC-100-900-2	0.21	0.13	0.00	0.78	1.00	0.55	0.64	8.43

The consistent growth of CPE_1-T corresponds to increasing of specific surface area and double-layer capacitance. The calculated values of CPE_2-P are in a range of about 0.39-0.45 for materials obtained at 600 °C and 0.36-0.55 for materials obtained at 900 °C that indicated the diffusion-controlled character of impedance. The deviation of CPE_2-P from 0.5 can be explained by the inhomogeneous distribution of pores and fractal structure of the electrode/electrolyte interface [30]. The presence of (R_3-C_3) chain was observed only for materials without mesopores structure and corresponds to non-homogeneous distributed capacitance of the EDL at the interface electrode/electrolyte. The dependence of the electrode potential on the CPE values indicates the weak specific adsorption of ions at different potential values and a change of surface charge density.

The typical cyclic voltammograms of synthesized carbons measured at two selected scan rates (30 mV/s) are shown in Fig. 8. The deviation of the CV curves from approximately rectangular shape indicates the presence of pseudocapacitance component both with the typical double-layer capacitance. Nevertheless the redox peaks correspond to surface faradaic were not clear observed. The very broadened anodic peaks are observed in the CV curves of samples obtained at 600 °C, but for samples obtained at 900 °C they practically are not observed. The pseudocapacitance may be caused by the nitrogen-contained groups on the surface of carbon particles which induce the complex faradic reactions in KOH aqueous solution [31]. The measured CV curves have a stable shape in a wide range of scan rates (1-50 mV/s) with proportional increasing of the peak area which indicate a good reversibility of kinetic process and the stability of electrode materials in aqueous electrolyte at different charging-discharging modes.

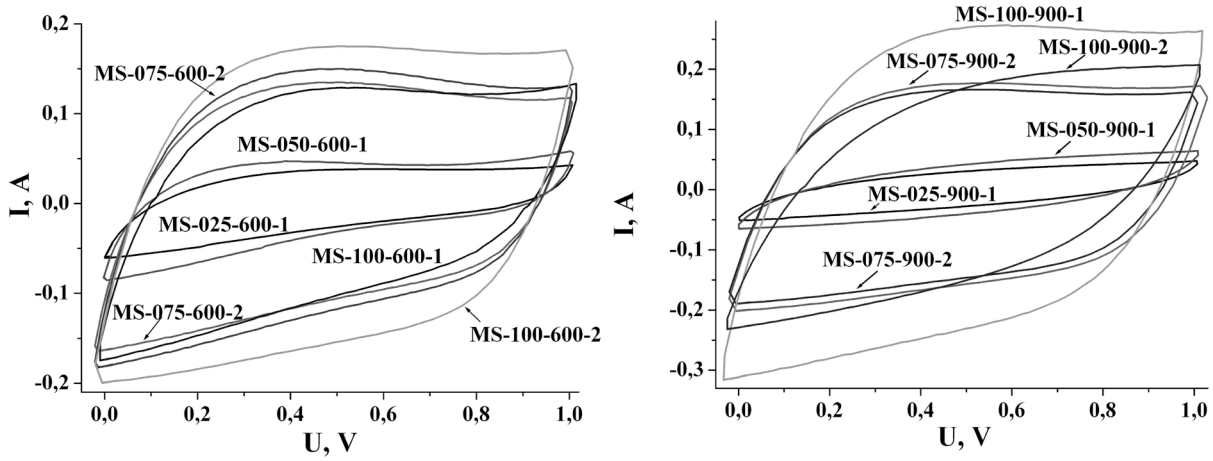

a) b)

Fig. 8. Typical cyclic voltammetry curves at a scan rate range of 30 mV/s for model capacitors based on carbons obtained (a) 600 and (b) 900 °C.

The curve shapes and the current plateaus increasing vary for different electrode materials in a same testing conditions (Fig. 8). The higher capacitance (plot area) was observed for materials with maximal amounts of micropores – samples of MC-075-600-2 and MC-100-900-1 for different series, respectively (Table 1). The different curve shapes clear indicated that the increasing of m(NaOH):m(C) weight ratio of leads to decreasing of charge current density thus indicate lower resistance to charge transfer of the carbon electrode. The specific capacitance *C* of the materials was calculated based on the CV measurements using the equation: $C = \int_{U_1}^{U_2} I(U)\,dU \Big/ 2ms(U_2 - U_1)$, where U_1 and U_2 are cutoff potentials in CV, $I(U)$ is an instantaneous current, *m* is a mass of individual sample, *s* is a scan rate [32].

Fig. 9 shows the specific capacitance values at different scan rates for model capacitors on the base of all the synthesized materials. All the cells show a common trend of capacitance decreasing at the scan rate increasing.

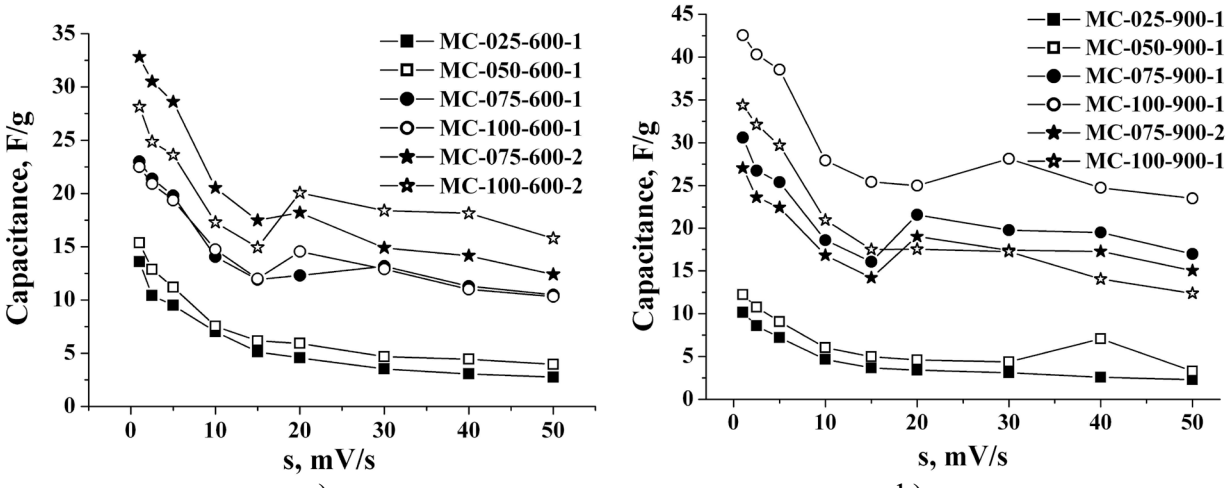

a) b)

Fig. 9. The specific capacitance (calculated from CV curves) versus scan rate for model capacitors based on carbons obtained at (a) 600 and (b) 900 °C.

The higher values of specific capacitance at low scan rates are caused by the mobility restriction of electrolyte ions and relatively longer time to its transfer through carbon material pores and electric double layer forming. In the scan rate region above 15 mV/s the specific capacitance values for materials obtained at 600 °C to decrease faster than that for carbons synthesized at 900 °C that is an evidence of the diffusion resistance increasing for ion transfer into the electrode pores. MC-100-900-1 material demonstrate the highest specific capacitance values throughout the whole with the

one of the lowest decreasing rate in a scan region of 15-50 mV/s. This result is in agreement with the EIS results about the highest value of CPE_1-T parameter which corresponds to capacitance of both double-layer and pseudocapacitance component. The using of cyclic voltammetry allows to separate non-Faradaic and Faradaic components and can also be used for calculation of carbon electrode's capacitance. These contributions can be separated using different kinetic dependence of each capacity on potential scan rate (s) [33]: $Q = Q_{s=\infty} + as^{-1/2}$ and $Q^{-1} = Q_{s=0}^{-1} + bs^{1/2}$, where Q is the total charge at different scan rates ($Q = Cm\Delta U = S/2s$, S is total area of CV curves), $Q_{s=\infty}$ is a double layer charge and $Q_{s=0}$ is the maximum total charge that can be obtained and a and b are constants. Experimental dependencies of $Q(s^{-1/2})$ and $Q^{-1}(s^{1/2})$ and also the results of their linear fitting are presented in Fig. 10.

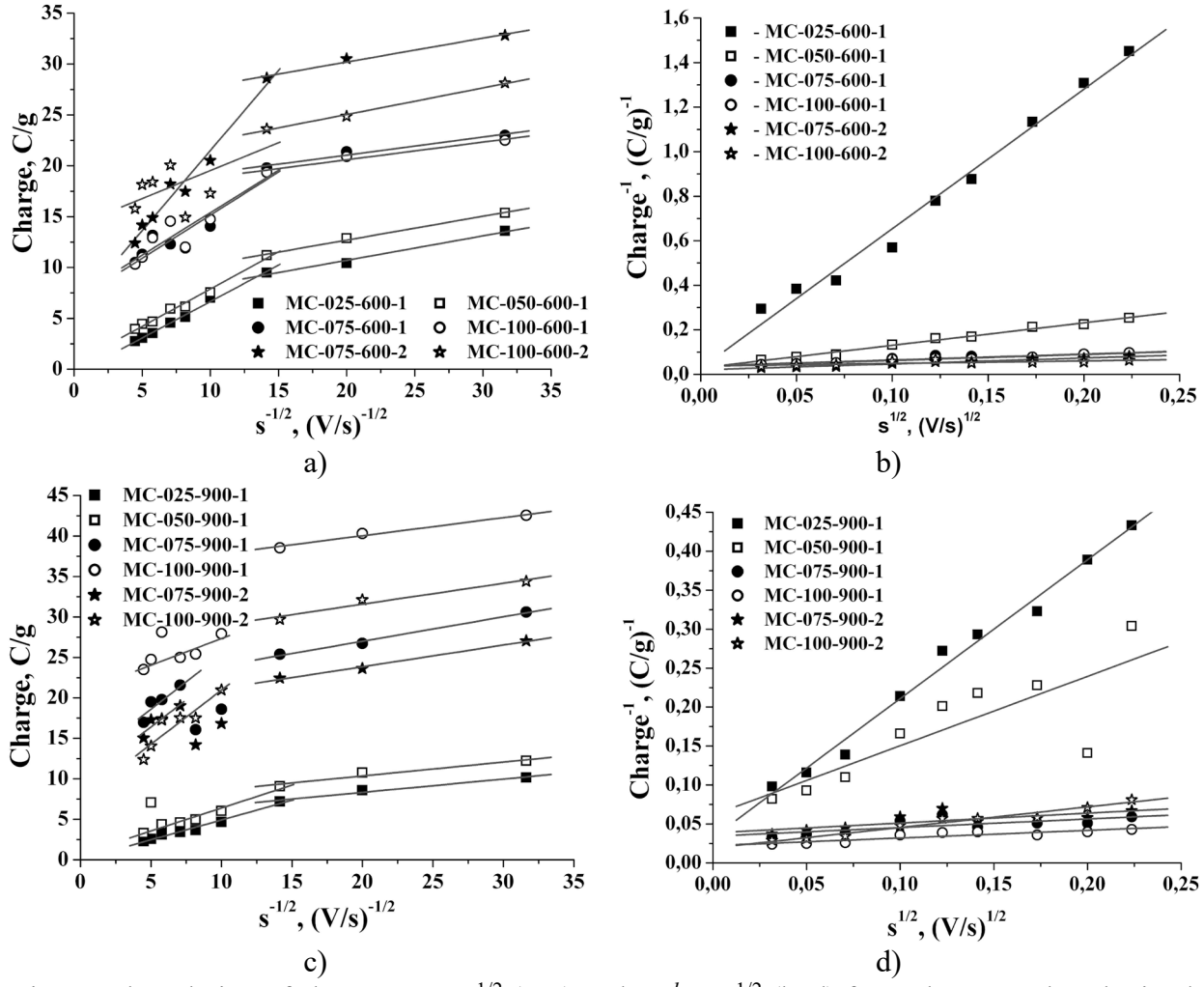

Fig.10. The relation of charge Q vs $s^{-1/2}$ (a, c) and Q^{-1} vs $s^{1/2}$ (b, d) for carbon samples obtained under different synthesis conditions.

Fig. 11 shows the contributions of the double layer capacitance to the total one of the carbon electrodes. For all the samples the double layer effects contribution to the total capacity is less than the diffusional ones. At the same time the decreasing of relative value of double layer capacitance corresponds to total capacitance increase (Fig. 11). This result indicates that the diffusional controlled reactions are very important to total capacitance formation. The highest capacitance value observed for MC-100-900-1 sample which have the lowest relative contribution of the double layer capacitance (about 54 %). This trend also is observed for samples obtained at 600 ºC where MC-075-600-2 sample have the highest contribution of pseudocapacitance (about to 33%). Some regularity of the diffusion-controlled redox capacitance contribution to the total one was found - the increasing of m(NaOH):m(C) weight ratio at samples synthesis causes the increasing of

pseudocapacitance contribution for once activated samples. At the same time the repeat of activation at the maximum value of activating agent concentration leads to decreasing of diffusional controlled reactions contribution. The presence of synergistic effect of NaOH concentration and number of activation procedures allows to control of total capacitance of carbon electrode.

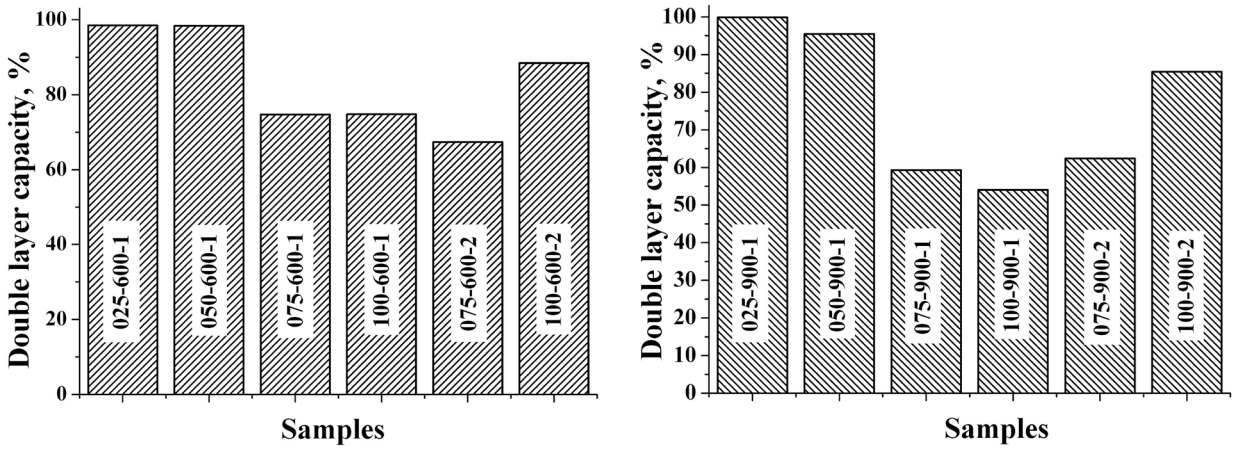

a) b)

Fig. 11. The average contributions of double layer capacity to the total capacitance of the carbon obtained at (a) 600 and (b) 900 ºC.

Specific capacitance and rate performance of carbon electrodes were calculated using cycling of model capacitors in galvanostatic charge-discharge mode at applied currents in a range of 1-100 mA/g in a potential window from -0.2 to 0.8 V. The typical charge-discharge curves measured at current density of 10 mA/g are shown in Fig. 12.

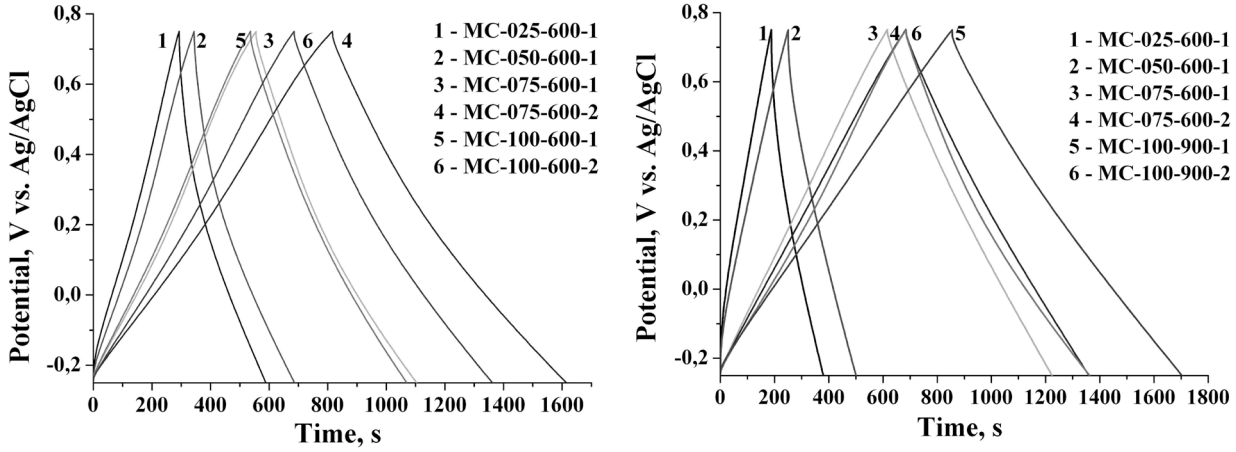

a) b)

Fig.12. Charge-discharge curves measured at current density of 50 mA/g for model capacitors based on carbons obtained at (a) 600 and (b) 900ºC.

The deformation on the charge-discharge curves in potential range 0.6-0.7 V is a result of pseudocapacitive redox processes and corresponds to reduction process previously identified by CV method. The discharge performance under the same conditions is better for carbons obtained at 900ºC. The specific capacitance of the synthesized carbons was calculated using the equation: $C_{spec} = I \cdot \Delta t / m \cdot \Delta U$, where I is a constant discharge current and Δt is the discharge time, m is the mass of electrode (g), ΔU is the potential window of discharge. The calculated values are shown in Fig. 13.

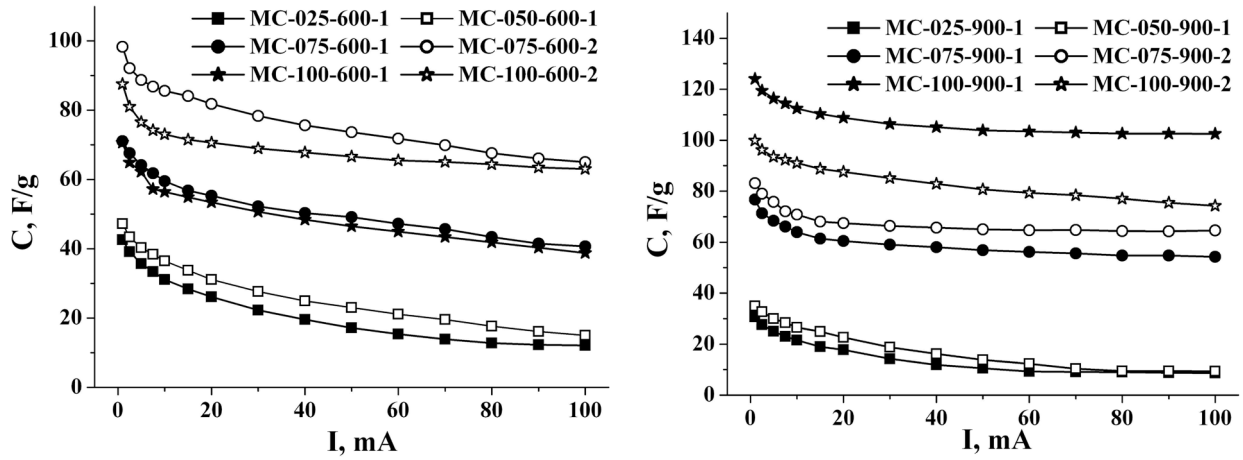

a) b)

Fig.13. The specific capacitance (calculated from galvanostatic charge-discharge cycling) versus current values for model capacitors based on carbons obtained at (a) 600 and (b) 900ºC.

Maximal value of specific capacity (up to about 100 F/g) for carbons obtained at 600ºC corresponds to MC-075-600-2 sample which is consistent with CV data. For samples obtained at 900ºC maximal specific capacitance (of about 120 F/g) was observed for MC-100-900-1 sample with the lowest rate of decrease in capacitance at current density increasing.

4. Conclusion

N-doped activated carbons were prepared by plant feedstock carbonization and chemical activation using NaOH. It was determined that both activation agent concentration and carbonization temperature effect on the porous structure and electrochemical performance of obtained carbons. The highest value of specific surface area (582 m^2g^{-1}) at simultaneous maximal relative contents of micropores (up to 95% of total area) observed for sample obtained at 900ºC after one activation procedure at m(NaOH):m(C)=1:1. The highest capacity value (calculated both from galvanostatic charge-discharge and voltammetry cycling) was observed for the samples with the low relative contribution of the double layer capacity that indicates the pseudocapacitance presence. It was found the increasing of m(NaOH):m(C) weight ratio at synthesis causes the increasing of redox capacitance contribution for once activated samples. The repeating of activation procedure results the decrease of diffusion controlled capacitance caused by the nitrogen-contained groups on the surface of carbon particles. The lowest average size of graphite nanocrystals was observed for double activated materials obtained at m(NaOH):m(C) weight ratio equals to 0.75. The maximal values of specific capacitance of carbon materials carbonized at 600ºC and 900ºC are about 100 and 120 F/g, respectively. The variation of activation agent concentration and the number of activation procedures allows controlling specific surface area and micropores relative content and predicting the contributions of double layer capacitance and diffusion-controlled redox capacitance to the total capacitance of microporous carbon.

References

[1] L.L. Zhang, X.S. Zhao, Chem. Carbon-based materials as supercapacitor electrodes, Soc. Rev. 38(9) (2009) 2520-2531.

[2] S. Arunachalam, B. Kirubasankar, E. Rajagounder Nagarajan, D. Vellasamy, S. Angaiah, A Facile Chemical Precipitation Method for the Synthesis of $Nd(OH)_3$ and $La(OH)_3$ Nanopowders and their Supercapacitor Performances, ChemistrySelect 3(45) (2018) 12719-12724.

[3] K. Singh, B. Kirubasankar, S. Angaiah, Synthesis and electrochemical performance of P2-$Na_{0.67}Al_xCo_{1-x}O_2$ ($0.0 \leq x \leq 0.5$) nanopowders for sodium-ion capacitors, Ionics 23(3) (2017) 731-739.

[4] B. Kirubasankar, P. Palanisamy, S. Arunachalam, V. Murugadoss, S. Angaiah, 2D $MoSe_2$-$Ni(OH)_2$ nanohybrid as an efficient electrode material with high rate capability for asymmetric supercapacitor applications, Chem. Eng. J.355 (2019) 881-890.
[5] S. Vijayan, B. Kirubasankar, P. Pazhamalai, A. K. Solarajan, S. Angaiah, Electrospun Nd^{3+}-Doped $LiMn_2O_4$ Nanofibers as High-Performance Cathode Material for Li-Ion Capacitors, ChemElectroChem 4(8) (2017). 2059-2067.
[6] K. Balakrishnan, M. Kumar, S. Angaiah, Adv. Mater. Res. 938 (2014) 51-157.
[7] S. Arunachalam, B. Kirubasankar, V. Murugadoss, D. Vellasamy, S. Angaiah, Facile synthesis of electrostatically anchored $Nd(OH)_3$ nanorods onto graphene nanosheets as a high capacitance electrode material for supercapacitors, New J. Chem. 42(4) (2018) 2923-2932.
[8] B. Kirubasankar, V. Murugadoss, J. Lin, T. Ding, M. Dong, H. Liu, S. Angaiah, In situ grown nickel selenide on graphene nanohybrid electrodes for high energy density asymmetric supercapacitors, Nanoscale 10(43) (2018) 20414-20425.
[9] B. Kirubasankar, S. Vijayan, S. Angaiah, Sonochemical synthesis of a 2D–2D $MoSe_2$/graphene nanohybrid electrode material for asymmetric supercapacitors, Sustainable Energy Fuels 3(2) (2019) 467-477.
[10] B. Kirubasankar, V. Murugadoss, S. Angaiah, Hydrothermal assisted in situ growth of CoSe onto graphene nanosheets as a nanohybrid positive electrode for asymmetric supercapacitors, RSC Adv. 7(10) (2017) 5853-5862.
[11] A. Subasri, K. Balakrishnan, E. R. Nagarajan, V. Devadoss, A. Subramania, Development of 2D $La(OH)_3$/graphene nanohybrid by a facile solvothermal reduction process for high-performance supercapacitors, Electrochim. Acta 281 (2018) 329-337.
[12] P.Yan, B. Zhang, KH Wu, D. Su, W. Qi, Surface chemistry of nanocarbon: Characterization strategies from the viewpoint of catalysis and energy conversion, Carbon 143 (2018) 915 - 936
[13] X. Huang, X. Yin, X. Yu, J. Tian, W. Wu, Preparation of nitrogen-doped carbon materials based on polyaniline fiber and their oxygen reduction properties, Colloids Surf., A 539 (2018) 163-170.
[14] B.K. Ostafiychuk, I.M. Budzulyak, M.M. Kuzyshyn, B.I. Rachiy, R.A. Zatorskiy, R.P. Lisovskiy, V.I. Mandzyuk, Nitrogen-containing nanoporous coal for electrodes of supercapacitors, J. Nano- Electron. Phys. 5 (2013) 03049-6.
[15] M.Y. Ghotbi, M. Azadfalah, Design of a layered nanoreactor to produce nitrogen doped carbon nanosheets as highly efficient material for supercapacitors, Mater. Des. 89 (2016) 708-714.
[16] Z.R. Ismagilov, A.E. Shalagina, O.Y. Podyacheva, A.V. Ischenko, L.S. Kibis, A.I. Boronin, Y.A. Chesalov, D.I. Kochubey, A. I. Romanenko, O.B. Anikeeva, T.I. Buryakov, E. N. Tkachev, Structure and electrical conductivity of nitrogen-doped carbon nanofibers, Carbon 47 (2009) 1922-1929.
[17] M. Demir, S.K. Saraswat, R.B. Gupta, Hierarchical nitrogen-doped porous carbon derived from lecithin for high-performance supercapacitors, RSC Advances 7 (2017) 42430-42442.
[18] Y. Wang, Y. Song, Y. Xia, Electrochemical capacitors: mechanism, materials, systems, characterization and applications, Chem. Soc. Rev. 45 (2016) 5925-5950.
[19] A.I. Kachmar, V.M. Boichuk, I.M. Budzulyak, V.O. Kotsyubynsky, B.I. Rachiy, R.P. Lisovskiy, Effect of synthesis conditions on the morphological and electrochemical properties of nitrogen-doped porous carbon materials, Fullerenes, Nanotubes, Carbon Nanostruct (2019).
[20] D. Corbett, N. Kohan, G. Machado, C. Jing, A. Nagardeolekar, B. Bujanovic, Chemical composition of apricot pit shells and effect of hot-water extraction, Energies 8(9) (2015).9640-9654.
[21] H. Li, Y. Qu, J. Xu, Microwave-assisted conversion of lignin, in: Zh. Fang, R. L. Smith Jr., X. Qi (Eds.), Production of biofuels and chemicals with microwave, Springer, Dordrecht, 2015, pp. 61-82.

[22] S.J. Gregg, K.S.W. Sing, Adsorption, surface area and porosity. London: Academic Press, 1982, 313 p.
[23] D. Johnson, Software Zview-v 2.3d, Scribner Associates Inc. (2000).
[24] L. Zou, B. Huang, Y. Huang, Q. Huang, C. A. Wang, An investigation of heterogeneity of the degree of graphitization in carbon–carbon composites, Mater. Chem. Phys. 82(3), (2003) 654-662.
[25] L. Bokobza, J. L. Bruneel, M. Couzi, Raman spectra of carbon-based materials (from graphite to carbon black) and of some silicone composites, C 1(1) (2015) 77-94.
[26] A.C. Ferrari, D.M. Basko, Raman spectroscopy as a versatile tool for studying the properties of graphene, Nat. Nanotechnol. 8 (2013) 235–246.
[27] M. A. Pimenta, G. Dresselhaus, M. S. Dresselhaus, L. G. Cancado, A. Jorio, R. Saito, Studying disorder in graphite-based systems by Raman spectroscopy, Phys. Chem. Chem. Phys. 9(11) (2007) 1276-1290.
[28] D.S. Yuan, J. Zeng, J. Chen, Y. Liu, Highly ordered mesoporous carbon synthesized via in situ template for supercapacitors, Int. J. Electrochem. Sci. 4(2009) 562-570.
[29] W. Sugimoto, H. Iwata, K. Yokoshima, Y. Murakami, Y. Takasu, Proton and electron conductivity in hydrous ruthenium oxides evaluated by electrochemical impedance spectroscopy: the origin of large capacitance, J. Phys. Chem. B 109 (2005) 7330-7338.
[30] B.B. García, F.M. Feaver, Q. Zhang, R.D. Champion, G. Cao, T.T. Fister, K.P. Nagle, G.T. Seidler, Effect of pore morphology on the electrochemical properties of electric double layer carbon cryogel supercapacitors, J. Appl. Phys. 104 (2008) 014305.
[31] G. Lota, E. Frackowiak, Pseudocapacitance effects for enhancement of capacitor performance, Fuel Cells 10(2010) 848-855.
[32] W. Chen, Z. Fan, L. Gu, X. Bao, C. Wang, Enhanced capacitance of manganese oxide via confinement inside carbon nanotubes, Chem. Commun. 46 (2010) 3905-3907.
[33] T. Nguyen, M. Boudard, M. Carmezim, M. Montemor, Layered $Ni(OH)_2$-$Co(OH)_2$ films prepared by electrodeposition as charge storage electrodes for hybrid supercapacitors, Sci. Rep. 7 (2017) 39980.